DART: Differentiable Dynamic Adaptive Region Tokenizer for Vision Transformer and Mamba

Shicheng Yin, Kaixuan Yin, Yang Liu, Weixing Chen, Liang Lin
Sun Yat-sen University, China

Abstract

Recently, non-convolutional models such as the Vision Transformer (ViT) and Vision Mamba (Vim) have achieved remarkable performance in computer vision tasks. However, their reliance on fixed-size patches often results in excessive encoding of background regions and omission of critical local details, especially when informative objects are sparsely distributed. To address this, we introduce a *fully differentiable* **Dynamic Adaptive Region Tokenizer (DART)**, which *adaptively partitions images into content-dependent patches of varying sizes*. DART combines learnable region scores with piecewise differentiable quantile operations to allocate denser tokens to information-rich areas. Despite introducing only approximately 1 million (1M) additional parameters, DART improves accuracy by 2.1% on DeiT (ImageNet-1K). Unlike methods that uniformly increase token density to capture fine-grained details, DART offers a more efficient alternative, achieving 45% FLOPs reduction with superior performance. Extensive experiments on DeiT, Vim, and VideoMamba confirm that DART consistently enhances accuracy while incurring minimal or even reduced computational overhead. Code is available at https://github.com/HCPLab-SYSU/DART.

1 Introduction

In recent years, Transformer-based models [1] have demonstrated strong potential in computer vision (CV) tasks. The Vision Transformer (ViT) [2] divides images into fixed-size patches and applies multi-head self-attention to model their relationships, as shown in Figure 1. However, due to the spatial redundancy commonly present in images [26], uniform patch partitioning may be suboptimal. This limitation can cause models to overlook important details, particularly when objects are small or scenes are visually complex.

Although increasing the sequence length by several times can substantially enhance token density and improve performance (highlighting the importance of fine-grained detail [27]), it comes at a high computational cost, exacerbating the redundancy of low-information regions. To balance fine-grained feature extraction with computational efficiency, hierarchical ViT structures such as PVT [3] and Swin [4] were proposed. They start with high patch density in the early stages and progressively downsample as token channels grow. As these models lack content awareness, they uniformly encode all regions at high resolution, then downsample and lose essential spatial information.

A natural idea is therefore to allocate finer resolution only to regions where it matters, saving computation on areas irrelevant to the task. We therefore propose **DART (Dynamic Adaptive Region Tokenizer)**, which adaptively partitions the input image before it reaches the backbone. Focusing on high-information regions with denser patches greatly improves detail retention, as shown in Figure 1. For example, simply adding DART to DeiT-Tiny [5] (224×224, 196 tokens) improves Top-1 accuracy by 2.1% on ImageNet-1K [13]. Unlike uniformly raising patch density, our local refinement cuts redundancy and delivers stronger performance at lower cost. Empirical results show that our dynamic partitioning significantly cuts down on overhead while boosting accuracy relative

Preprint. Under review.

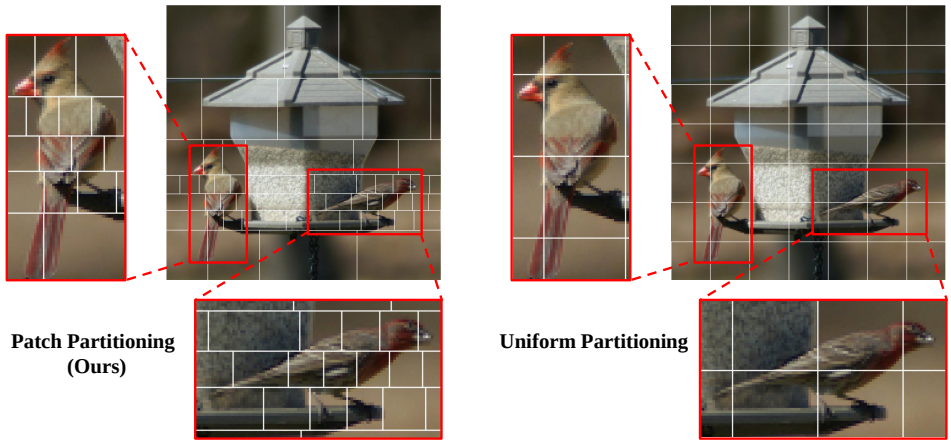

Figure 1: Comparison between our patch partitioning (left) and the uniform partitioning (right). Finer patches are allocated to the bird region, merging low-information background.

to a "long-sequence" fine-tuning approach that uniformly increases patch density. For example, Vim [12] uses four times the sequence length to achieve better fine-grained detail, whereas our method (with only twice the sequence length) surpasses that performance at roughly half the FLOPs. In Vim-Tiny, we reduce FLOPs by 45% yet still gain a 0.6% accuracy increase (shown in Figure 2), underscoring the inefficiency of uniformly extending patch density in regions of low information.

Core Steps. The core steps of our method are: 1) Use a partially pretrained lightweight network to extract features and learn region importance scores, 2) Perform piecewise differentiable quantile operations to partition the image into non-uniform patches, 3) Resample each patch area to a fixed size via bilinear interpolation, enabling a drop-in replacement for the conventional fixed-size patch tokenizer. We treat the positional embeddings as an $H \times W \times D$ feature map and apply the same transformation. Our contributions can be summarized as follows:

- We introduce a fully differentiable Dynamic Adaptive Region Tokenizer (DART) module that adaptively partitions the image by combining learnable region scores with piecewise differentiable quantile operations.
- We validate the DART module on DeiT, Vim, and VideoMamba, demonstrating consistent performance improvements with minimal or even reduced computational overhead.

2 Related Work

2.1 Vision Transformers and Improvements

ViT [2] established a pure Transformer for classification, catalyzing research on Transformer-based vision models [1]. Despite strong results, ViT typically needs large-scale data and uses rigid patch splitting. DeiT [5] mitigated data demands via distillation and augmentation yet still suffers uniform partitioning. Our DART tackles this by dynamically adjusting patches.

2.2 Dynamic Adaptive Inference for Vision

In recent years, numerous dynamic token-processing techniques [30] have emerged to enhance a vision model's ability to adaptively handle input tokens. These methods select, merge, or discard patches/tokens based on their content importance to accelerate inference and reduce computation. For instance, DynamicViT [6] introduced a lightweight prediction network that assigns scores to each token and discards tokens of lower importance, thereby cutting FLOPs by around 35% at the cost of about 0.5% accuracy. Pan et al. proposed IA-RED^2 [7], removing redundant tokens for improved efficiency. Similarly, A-ViT [8] employed an auxiliary module to predict token importance and prune unimportant tokens. Such score-based dynamic partitioning methods typically rely on

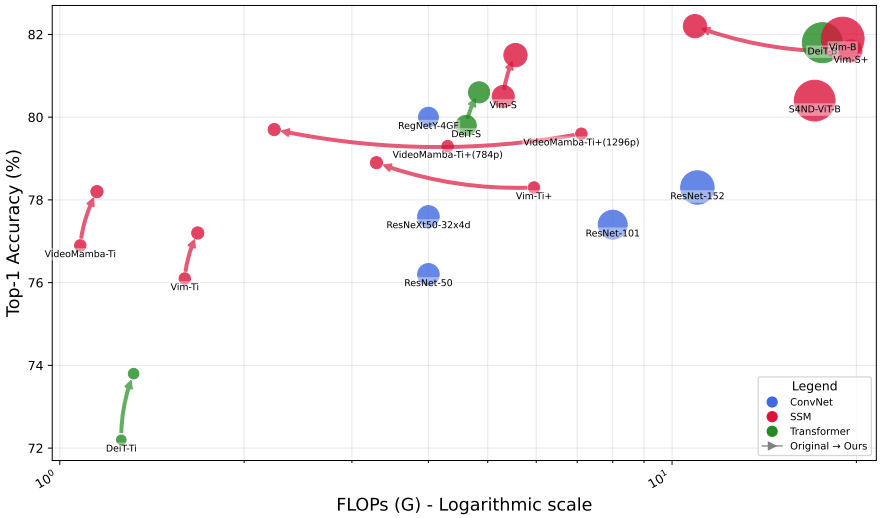

Figure 2: Accuracy-FLOPs curves on the ImageNet-1K validation set for various models. Circle size denotes parameter count. Arrows represent adding our DART: the starting point is the baseline, and the endpoint is with DART.

feedforward networks or extra attention mechanisms to model token importance, adjusting the token count according to the input.

We also focus on dynamic token processing here but implement it before the Transformer backbone, at the tokenizer stage, rather than pruning or merging tokens within a standard Transformer block. Our approach decouples dynamic partitioning from the specific backbone, making it applicable to popular architectures such as the Mamba [10] family.

In CV, several studies have investigated differentiable selection mechanisms for end-to-end learning of key regions. For instance, Cordonnier et al. [9] proposed Differentiable Patch Selection, which employs a differentiable Top-K operator to retain only the most relevant patches from a high-resolution image. The selected K patches are processed independently by the backbone, and their outputs are subsequently aggregated.

2.3 Mamba Architectures for Vision and Dynamic Input Adaptation

State Space Models (SSMs) have recently gained attention as a promising alternative for long-sequence modeling, with the potential to replace Transformers. A representative example is Mamba [10], which introduces selection mechanisms via S6 modules in continuous state space to enable linear-time processing of very long sequences, achieving strong performance in language modeling. However, applying SSMs to vision tasks requires an effective approach to handle 2D image inputs. An early attempt by Gu et al. [11] proposed S4, which offers efficient sequence representations but flattens images into 1D sequences, thereby disrupting spatial structure. To address this limitation, researchers have developed several vision-oriented extensions of Mamba. For example, Zhu et al. [12] introduced Vim, a bidirectional state space model that processes image patches in both forward and backward directions to alleviate the mismatch between 1D scanning and 2D spatial layout. Experiments show that Vim can match ViT-level performance in classification and detection tasks without relying on self-attention, demonstrating the potential of SSMs in vision applications.

Nevertheless, these vision SSM extensions typically rely on fixed patch partitioning and scanning strategies, limiting their adaptability to diverse image content. Experiments with Vim show that simply appending our dynamic partitioning module before Vim's bidirectional SSM blocks leads to significant performance improvements.

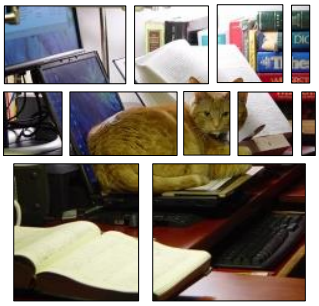

(a) Example of dynamic patch partitioning.

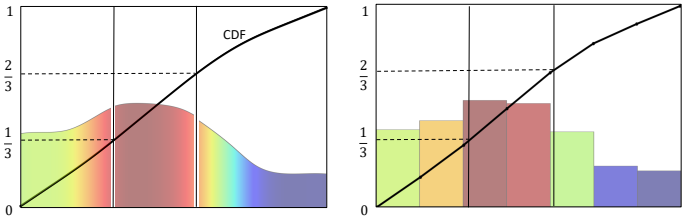

(b) Illustration of differentiable quantile computation. The histogram-like distribution and the piecewise linear CDF are shown.

Figure 3: The schematic of the non-uniform patch partitioning.

3 Method

Figure 3a depicts a schematic of the non-uniform patch partitioning produced by our dynamic tokenizer module, resembling tiles on a wall. The overall process can be summarized as follows.

3.1 Feature Extraction and Entropy Score Computation

Given an input image $X \in \mathbb{R}^{H\times W\times 3}$, we first rescale it to a fixed size (e.g., 448×448). To efficiently extract shallow features in an end-to-end manner, we employ a pretrained lightweight convolutional network (e.g., the first 11 layers of MobileNetV3-Small [16] or another compact model) to process the image, generating $F \in \mathbb{R}^{H'\times W'\times C}$. Here, $H' = H/4$ and $W' = W/4$, with C denoting the channel dimension. To further reduce computational cost, a lower input resolution (e.g., 224×224) can also be used.

We obtain the score matrix $\{s_{i,j}\}$, normalize it across batch and within each sample, and then apply a sigmoid to constrain the values to the range [0,1]. Subsequently, we perform an additional normalization within each sample to ensure that the spatial scores in a single image sum to 1, resulting in $\tilde{s}_{i,j}$, which serves as a 2D probability distribution over the feature map.

3.2 Differentiable Patch Partitioning Strategy

To enable adaptive vertical and horizontal patch partitioning in an end-to-end manner, we design a differentiable quantile computation that determines image partition boundaries, shown in Figure 4.

Consider a finite discrete probability distribution S, without loss of generality defined on integer points of length seqlen. Suppose the non-zero portion starts at 0 and ends at seqlen: $S = \{S_i\}_{i=0}^{\text{seqlen}-1}$. We first convert this discrete distribution into a piecewise-constant function X:

$$f_X(x) = \begin{cases} S_i, & x \in (i, i+1], \quad i = 0, 1, 2, \ldots, \text{seqlen} - 1 \\ 0, & \text{otherwise.} \end{cases} \tag{1}$$

This distribution looks like a histogram of seqlen equally wide bars. Its cumulative distribution function (CDF) is a piecewise-linear, monotonically increasing curve with seqlen segments. The CDF's inverse is also piecewise linear, making it straightforward to compute the seqlen $-$ 1 *uniform quantiles* $x_{1/\text{seqlen}}, x_{2/\text{seqlen}}, \ldots$. By using these quantile points as boundaries, we can divide the distribution into seqlen intervals. Since the CDF's inverse is piecewise linear and differentiable almost everywhere, these quantile points are almost everywhere differentiable with respect to S (as shown in Figure3b).

Given a 2D discrete score distribution $\{S_{i,j}\}_{i=0,j=0}^{\text{seqlen}-1}$ obtained by the scoring network, we first compute its *marginal distribution* in one dimension and apply the same continuous method described above. Because Vim scans row-major, we first compute the y-dimensional marginal and apply 1D quantile splitting for equally integrated segments, yielding rows of varying heights. For the next step, which is identifying vertical boundaries, we concatenate these rows in sequence. Each row's new 2D

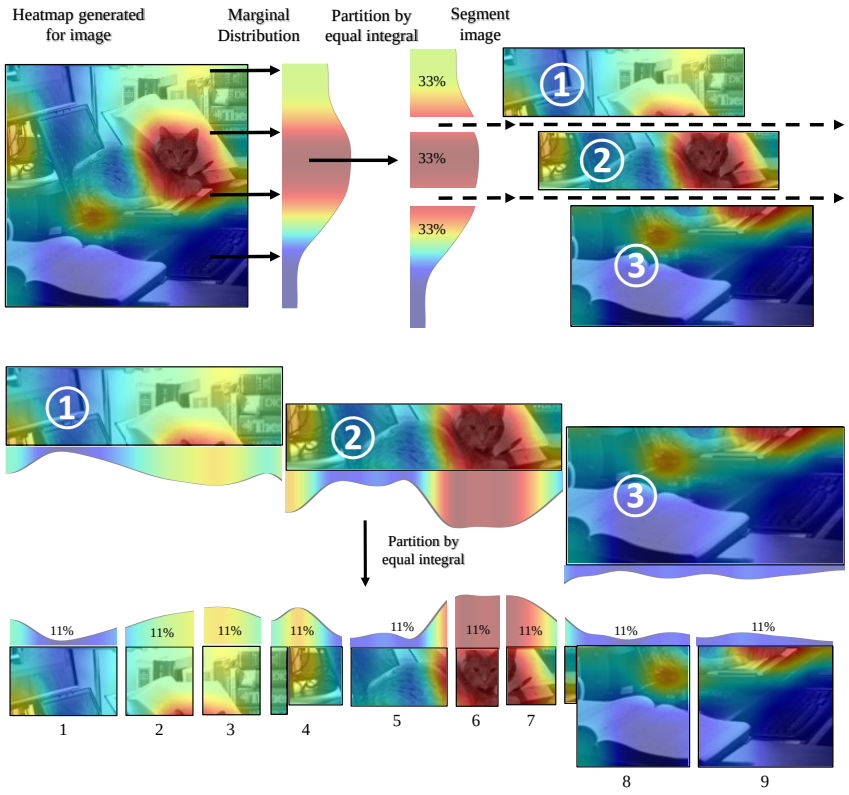

Figure 4: Illustration of differentiable patch partitioning via quantiles, using samples from ImageNet. Both horizontal and vertical partitioning steps are shown, where the score map produced by the lightweight network is overlaid on the image.

distribution can be derived by a linear combination of the original distributions. We then compute the marginal distribution in the new coordinate system along the x dimension, again partition it into seqlen segments by quantiles, and obtain the final patch divisions.

When the distribution is uniform, our partitioning degenerates to the standard ViT's fixed partitioning, ensuring full compatibility.

3.3 Video Patch Partitioning Strategy

Our approach also applies to video tasks. Figure 5 presents an example of patch partitioning on a sample from the SSv2 dataset. Specifically, we vertically concatenate all input frames into one tall image and then perform our dynamic partitioning on this concatenated image. This allows a limited token sequence length to be unevenly allocated across different frames, focusing computational resources on key frames. Besides spatial redundancy (as in images), videos also exhibit *temporal redundancy*, where the same objects can be redundantly encoded in multiple frames. Hence, our scoring network must reflect not only spatial but also temporal information density. In our implementation, we simply compute the difference between feature maps of consecutive frames and feed it (together with the global pooled feature) into the scoring network. This approach avoids repeatedly encoding static objects at high density across multiple frames, and it can better capture subtle motions compared to naive pixel-difference methods.

3.4 Patch Resampling and Projection

Once we obtain the coordinate region for each patch, we use bilinear interpolation to resample that patch to a fixed size (e.g., 16×16), yielding a tensor $P_k \in \mathbb{R}^{16\times16\times3}$. The 16×16 grid of interpolation points is derived from the rectangle defined by the partitioning step, ensuring that the resampling

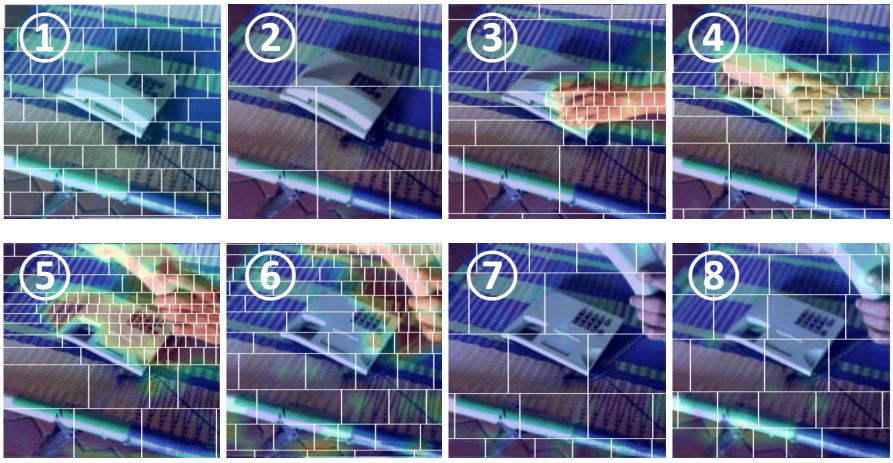

Figure 5: Patch partitioning on an example from the SSv2 dataset.

remains differentiable with respect to the region scores. Next, as in standard ViT/Vim, we apply a linear projection to P_k and add learnable positional embeddings, forming the token T_k. We adjust embeddings to each token's size and location, keeping the sequence length(e.g. 196) but with tokens covering different spatial areas.

3.5 Loss Function and Training

Because our patch partitioning strategy is piecewise differentiable, we can train the entire system end-to-end together with the subsequent backbone (e.g., DeiT, Vim) without any additional supervision. We use the same loss as in standard image classification, such as cross-entropy. The network learns an appropriate region scoring distribution and optimal partitioning strategy to best utilize a limited number of tokens for capturing crucial local information.

3.6 Model Complexity Analysis

Both the partitioning and resampling steps can be efficiently parallelized on a GPU and thus incur roughly constant overhead. The lightweight model used for preliminary feature extraction adds negligible compute cost relative to the main backbone, allowing us to preserve nearly the same FLOPs and computational complexity as the baseline model.

4 Experiments

4.1 Experimental Setup

We evaluate on ImageNet ILSVRC-2012 [13] (1.28M training images, 50k validation). Top-1 accuracy is our primary metric.Our baselines include the advanced and canonical DeiT architecture, as well as the more recent Mamba-based Vim and the minimal yet high-performance VideoMamba [14]. In addition, to verify our tokenizer's potential in downstream tasks, we use VideoMamba with the Something-Something V2 (SSv2) [15] dataset for video classification, again evaluating Top-1 accuracy. All experiments are run on a single machine equipped with eight NVIDIA A100 GPUs. All training hyper-parameters strictly follow the public configurations of the respective baselines.

4.2 Experiments on DeiT

We follow the DeiT training setup exactly, using AdamW [23] for 300 epochs with linear learning-rate scaling. The base learning rate is 1e-3 for a 1024 batch size, paired with cosine decay [24] and a 5-epoch warm-up. To avoid extra training data, we freeze a MobileNetV3 model pretrained on ImageNet-1K and feed its intermediate-layer output into a small two-layer MLP (reducing to 1 dimension) to generate region scores.

Table 1: Comparison of ImageNet results. † denotes long-sequence fine-tuning.

Backbone	Tokenizer	Params (M)	Patches	GFLOPs	Top-1 (%)
Transformers					
DeiT-Ti [5]		6	196	1.26	72.2
DeiT-Ti	**DART**	7	196	1.32	73.8 **(+1.6)**
DeiT-S [5]		22	196	4.61	79.8
DeiT-S	**DART**	24	196	4.84	80.6 **(+0.8)**
DeiT-S†		22	576	15.5	81.6
DeiT-S†	**DART**	24	**392**	10.1**(-35%)**	81.8 **(+0.2)**
SSMs					
Vim-Ti [12]		7	196	1.60	76.1
Vim-Ti	**DART**	8	196	1.68	77.2 **(+1.1)**
Vim-S [12]		26	196	5.30	80.5
Vim-S	**DART**	29	196	5.55	81.5 **(+1.0)**
VideoMamba-Ti		7	196	1.08	76.9
VideoMamba-Ti	**DART**	8	196	1.15	78.2 **(+1.3)**
Vim-Ti† [12]		7	784	5.95	78.3
Vim-Ti†	**DART**	8	**392**	3.29 **(-45%)**	78.9 **(+0.6)**
Vim-S† [12]		26	784	19.6	81.6
Vim-S†	**DART**	29	**392**	10.9 **(-44%)**	82.2 **(+0.6)**
VideoMamba-Ti†		7	784	4.30	79.3
VideoMamba-Ti†		7	1296	7.11	79.6
VideoMamba-Ti†	**DART**	8	**392**	2.24 **(-69%)**	79.7 **(+0.1)**

Table 2: Comparison with prior works on dynamic inference for DeiT.

Model	Patches	GFLOPs	Acc. (%)
A-ViT-T	dynamic	0.8	71.0
DeiT-Ti +DART	**121**	**0.8**	**71.8**
DeiT-Ti +DART	**196**	**1.3**	**73.8**
DeiT-S	196	4.61	79.8
DeiT-S 384	576	15.5	81.6
DynamicViT-S/0.5	dynamic	7.0	80.3
A-ViT-S	dynamic	3.6	78.6
DeiT-S +DART	**144**	**3.6**	**79.9**
DeiT-S +DART	**196**	**4.8**	**80.6**
DeiT-S +DART	**288**	**7.2**	**81.5**
DeiT-S +DART	**392**	**10.1**	**81.8**
DeiT-B	196	17.5	81.8
DynamicViT-B/0.7	dynamic	11.2	81.3
DeiT-Base +IA-RED^2	dynamic	11.8	80.3

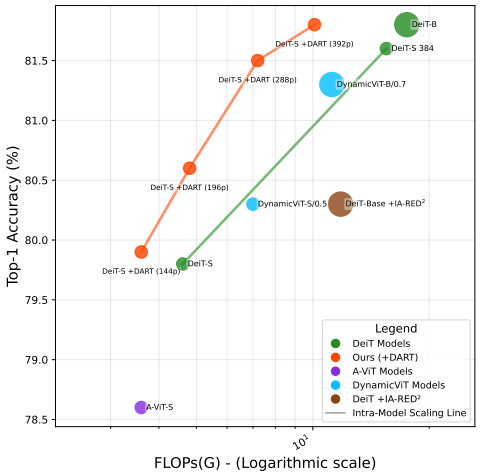

Figure 6: Model performance plot. Marker size indicates parameter count.

Table 1 shows the DeiT results. With the dynamic tokenizer, *DeiT-Tiny* improves Top-1 accuracy by 1.6%, with only about 1M more parameters and a negligible difference in FLOPs. This indicates that under a fixed sequence length and similar compute, our method better captures details and sparse objects. Table 2 and Figure 6 compare our approach with previous dynamic-inference methods on DeiT and trace how accuracy and FLOPs evolve as the patch count scales. As the figure shows, the setting with 392 patches emerges as a sweet spot that balances computational cost and accuracy. Overall, our method achieves a more favorable efficiency–accuracy trade-off than existing techniques.

4.3 Experiments on Vim

Vision Mamba (Vim) [12] replaces standard self-attention with Mamba blocks, achieving $O(N)$ linear complexity for a sequence of length N. However, if the input resolution is high, N can still be large.

Table 3: Video classification task. * denotes our baseline model trained under the same conditions using the official repository code.

Method	Params (M)	Patches	GFLOPs	Top-1 (%)
VideoMamba-Ti*	7	196×8	8.60	63.2
+DART	8	196×4	5.11 **(-41%)**	63.7 **(+0.5)**

Table 4: Comparison of ImageNet results under various pretrained scoring backbones.

Networks	Params (M)	FLOPs	Top-1 (%)
w/o (baseline)	6	1.26	72.2
MobileNetV3 Small	7	1.32	73.8 **(+1.6)**
MnasNet [18]	7	1.37	74.0 **(+1.8)**
SqueezeNet [17]	7	1.54	74.3 **(+2.1)**
EfficientNet-B0 [19]	10	2.41	75.1 **(+2.9)**

Table 1 presents our experimental results on Vim. Without altering Vim's original layers or sequence length, we swap its fixed-size tokenizer for our dynamic tokenizer. This delivers better recognition in key areas at comparable compute. Specifically, we freeze a MobileNetV3-Small model pretrained on ImageNet-1K, take the feature maps from its first 13 layers, apply global average pooling, and pass the result through a two-layer MLP. The MLP output is then multiplied with the feature vector at every spatial location to generate region scores, which are used to perform a differentiable, dynamic partitioning of the image.

Despite the Mamba architecture's design being quite distinct from Transformers and already offering efficient selective scanning, our method still achieves a notable 1.1% improvement, highlighting its broad compatibility. In Vim, extending the sequence length to four times the default during fine-tuning enhances fine-grained detail, but incurs substantial computational cost. Leveraging our tokenizer's dynamic compression, we apply denser partitioning only where necessary, significantly reducing redundant encoding in uninformative regions. With just a $2\times$ longer sequence (instead of $4\times$), our approach surpasses the $4\times$ baseline while using approximately half the FLOPs, yielding an additional +0.6% in Top-1 accuracy. As shown in Table 1, our dynamic partitioning mechanism and linear Mamba blocks complement each other effectively.

4.4 Experiments on VideoMamba

VideoMamba [14] is a recent video model entirely based on Mamba. Its backbone is pretrained on ImageNet-1K for image classification and demonstrates performance gains over Vim. Similar to Vim, we apply DART to VideoMamba for pretraining, achieving a 1.3% improvement in validation accuracy compared to the baseline, as shown in Table 3. Compared to the reported long-sequence fine-tuning baseline, our approach achieves higher accuracy while reducing FLOPs by approximately 70%, highlighting the broad applicability of our method. Following VideoMamba's training protocol, we further fine-tune the model on the SSv2 video dataset and again observe improved accuracy using only half the sequence length. Aside from the integration of DART, all training configurations remain unchanged. For feature extraction, we use the first 8 layers of MobileNetV3-Small pretrained on ImageNet-1K. We compute feature differences between consecutive frames and combine them with globally average-pooled features. These are passed through fully connected layers and activation functions, followed by element-wise multiplication to produce the final score distribution. This design prevents the redundant encoding of static objects across multiple frames.

5 Ablation Studies

5.1 Impact of the Score Generation Network

We conduct experiments on DeiT-Tiny, replacing the intermediate-layer output of MobileNetV3-Small with various other small networks pretrained on ImageNet-1K as inputs for our score-generation module. As shown in Table 4, we obtain similar performance gains at comparable parameter scales. For instance, using SqueezeNett [17] yields an additional 0.5% improvement over the baseline, a total

Figure 7: Visualization of dynamic partitioning across different training epochs. We overlay the learned score heatmap along with the resulting patch boundaries. Over time, the model focuses on the relevant region of interest and refines its patch subdivisions accordingly.

of +2.1%. With the slightly larger EfficientNet-B0, we see an even bigger boost of +2.9%. These ablations confirm that stronger pretrained feature extractors yield better region scores and higher accuracy, allowing us to balance cost and partitioning quality by adjusting the scoring network's capacity.

Although Mamba's selective scanning provides linear complexity and stronger global context, it can face "forgetting" issues over extremely long contexts compared to Transformer self-attention. Consequently, using a simple MLP-based scoring (as in DeiT) showed instability when training with Vim or VideoMamba. Thus, for Vim (and VideoMamba), we use a more complex scoring extractor, specifically the first 13 layers of MobileNetV3-Small pretrained on ImageNet-1K, followed by global average pooling [25] and a two-layer MLP to compute region scores via elementwise multiplication with the feature map. To analyze this effect, we tried the same "Vim" scoring extractor on DeiT-Tiny, finding near-identical performance (73.7%, which is 0.1% lower) to the simpler MLP-based approach. This shows that, for Transformers, a simpler design often suffices.

Overall, these experiments suggest that our method is robust to various pretrained feature extraction networks and architectural choices.

When the score-generation network produces a uniform distribution, our partitioning reverts exactly to standard ViT. Since we introduce no other changes to the experimental configuration aside from adding DART, the performance gains relative to the baseline can be fairly attributed to our dynamic partitioning approach.

5.2 Training Dynamics of Differentiable Partitioning

Owing to our differentiable patch-partitioning design, the tokenizer automatically learns to segment tokens in a manner that preserves informative content for the backbone—without requiring any additional supervision. The ImageNet classification loss is directly backpropagated into the score-generation network. As shown in Figure 7, the patch density distribution appears chaotic during early training. However, due to the differentiability of the horizontal and vertical boundaries, they can effectively "slide" across the image. Over time, the partitioning converges to a more semantically meaningful token distribution that enhances downstream classification performance.

6 Limitations

While our DART integrates seamlessly with sequence-based models, extending it to CNN-hybrid architectures, which inherently operate on a uniform convolutional grid, requires additional adaptation. As demonstrated in our DeiT-Ti ablations, selecting a more suitable lightweight feature extractor, such as replacing MobileNetV3 with SqueezeNet, results in a 0.5% improvement in accuracy. Moreover, adopting a more powerful backbone (e.g., EfficientNet) leads to even greater performance gains. Although end-to-end fine-tuning may yield further improvements, we freeze the feature extraction network for simplicity. Finally, although DART shows promise in tasks involving sparse targets or fine-grained details (e.g., ultra-high-resolution images or fine-grained classification), we focus on ImageNet to ensure a fair comparison with existing dynamic inference approaches.

7 Conclusion

We present DART, a method that adaptively partitions image patches based on information density, providing resolution in critical regions. Without modifying the main backbones such as ViT or Vim, simply inserting our lightweight module at the tokenizer stage achieves notable accuracy improvements on ImageNet and offers more flexible modeling of sparse targets and fine details. Future work includes incorporating our adaptive tokenizer into object detection, video understanding, and multimodal tasks to further exploit its potential and utility.

References

[1] A. Vaswani, N. Shazeer, N. Parmar, J. Uszkoreit, L. Jones, A.N. Gomez, L. Kaiser, and I. Polosukhin. Attention is all you need. In *Advances in Neural Information Processing Systems*, 2017.

[2] A. Dosovitskiy, L. Beyer, A. Kolesnikov, et al. An image is worth 16x16 words: Transformers for image recognition at scale. In *International Conference on Learning Representations (ICLR)*, 2021.

[3] W. Wang, E. Xie, X. Li, et al. Pyramid vision transformer: A versatile backbone for dense prediction without convolutions. In *Proceedings of the IEEE/CVF International Conference on Computer Vision (ICCV)*, 2021.

[4] Z. Liu, Y. Lin, Y. Cao, et al. Swin transformer: Hierarchical vision transformer using shifted windows. In *Proceedings of the IEEE/CVF International Conference on Computer Vision (ICCV)*, 2021.

[5] H. Touvron, M. Cord, M. Douze, et al. Training data-efficient image transformers & distillation through attention. In *International Conference on Machine Learning (ICML)*, 2021.

[6] Y. Rao, J. Wang, Z. Zhang, et al. DynamicViT: Efficient vision transformers with dynamic token sparsification. In *Advances in Neural Information Processing Systems*, 2021.

[7] T. Pan, R. Xu, Y. Shen, et al. IA-RED^2: Interpretability-aware redundancy reduction for vision transformers. In *Proceedings of the IEEE/CVF Conference on Computer Vision and Pattern Recognition (CVPR)*, 2022.

[8] H. Yin, A. Vahdat, J.M. Alvarez, et al. A-ViT: Adaptive tokens for efficient vision transformer. In *Proceedings of the IEEE/CVF Conference on Computer Vision and Pattern Recognition (CVPR)*, 2022.

[9] J.-B. Cordonnier, A. Mahendran, A. Dosovitskiy, et al. Differentiable patch selection for image recognition. In *Proceedings of the IEEE/CVF Conference on Computer Vision and Pattern Recognition (CVPR)*, 2021.

[10] A. Gu and T. Dao. Mamba: Linear-Time Sequence Modeling with Selective State Spaces. In *arXiv preprint arXiv:2312.00752*, 2023.

[11] A. Gu, K. Goel, and C. Ré. Efficiently modeling long sequences with structured state spaces. In *International Conference on Learning Representations (ICLR)*, 2022.

[12] L. Zhu, B. Liao, X. Wang, et al. Vision Mamba: Efficient Visual Representation Learning with Bidirectional State Space Model. In *arXiv preprint arXiv:2401.09417*, 2024.

[13] J. Deng, W. Dong, R. Socher, et al. ImageNet: A large-scale hierarchical image database. In *Proceedings of the IEEE Conference on Computer Vision and Pattern Recognition (CVPR)*, 2009.

[14] Y. Li, J. Wang, Y. Dai, et al. VideoMamba: State Space Model for Efficient Video Understanding. In *arXiv preprint arXiv:2403.06753*, 2024.

[15] R. Goyal, M. Easetvveood, M. Ebrahimi, et al. The Something Something Datasets for Learning Collection of Composable Actions. In *Proceedings of the IEEE International Conference on Computer Vision (ICCV)*, 2017.

[16] A. Howard, M. Sandler, G. Chu, et al. Searching for MobileNetV3. In *Proceedings of the IEEE/CVF International Conference on Computer Vision (ICCV)*, 2019.

[17] F.N. Iandola, S. Han, M.W. Moskewicz, et al. SqueezeNet: AlexNet-level accuracy with 50x fewer parameters and <0.5MB model size. In *arXiv preprint arXiv:1602.07360*, 2016.

[18] M. Tan, B. Chen, R. Pang, et al. MnasNet: Platform-Aware Neural Architecture Search for Mobile. In *Proceedings of the IEEE/CVF Conference on Computer Vision and Pattern Recognition (CVPR)*, 2019.

[19] M. Tan and Q.V. Le. EfficientNet: Rethinking Model Scaling for Convolutional Neural Networks. In *International Conference on Machine Learning (ICML)*, 2019.

[20] G. Hinton, O. Vinyals, and J. Dean. Distilling the knowledge in a neural network. In *arXiv preprint arXiv:1503.02531*, 2015.

[21] E.D. Cubuk, B. Zoph, J. Shlens, et al. Randaugment: Practical automated data augmentation with a reduced search space. In *Proceedings of the IEEE/CVF Conference on Computer Vision and Pattern Recognition Workshops (CVPRW)*, 2020.

[22] K. He, X. Zhang, S. Ren, and J. Sun. Deep residual learning for image recognition. In *Proceedings of the IEEE Conference on Computer Vision and Pattern Recognition (CVPR)*, 2016.

[23] I. Loshchilov and F. Hutter. Decoupled weight decay regularization. In *International Conference on Learning Representations (ICLR)*, 2019.

[24] I. Loshchilov and F. Hutter. SGDR: Stochastic gradient descent with warm restarts. In *International Conference on Learning Representations (ICLR)*, 2017.

[25] M. Lin, Q. Chen, and S. Yan. Network in network. In *arXiv preprint arXiv:1312.4400*, 2013.

[26] K. Tong, Y. Wu, F. Zhou, et al. Recent advances in small object detection based on deep learning: A review. In *Image and Vision Computing*, 2020.

[27] X.-S. Wei, C.-W. Xie, J. Wu, and C. Shen. A Survey on Deep Learning for Fine-Grained Image Categorization and Retrieval. In *ACM Computing Surveys (CSUR)*, 2021.

[28] L. Yuan, Y. Chen, T. Wang, et al. Tokens-to-token vit: Training vision transformers from scratch on imagenet. In *Proceedings of the IEEE/CVF International Conference on Computer Vision (ICCV)*, 2021.

[29] X. Chu, Z. Tian, Y. Wang, et al. Conditional positional encodings for vision transformers. In *International Conference on Learning Representations (ICLR)*, 2021.

[30] Z. Zhang, P. Song, K. Wang, and L. Zhang. A survey on dynamic token in vision transformer. In *arXiv preprint arXiv:2312.11202*, 2023.

[31] I. Radosavovic, R.P. Kosaraju, R. Girshick, K. He, and P. Dollár. Designing network design spaces. In *Proceedings of the IEEE/CVF Conference on Computer Vision and Pattern Recognition (CVPR)*, 2020.

[32] S. Xie, R. Girshick, P. Dollár, Z. Tu, and K. He. Aggregated residual transformations for deep neural networks. In *Proceedings of the IEEE/CVF Conference on Computer Vision and Pattern Recognition (CVPR)*, 2017.

Table 5: Feature extractors

Model	Feature Extractor
DeiT-Ti	MobileNetV3 Small[:11]
DeiT-S	MobileNetV3 Large[:15]
Vim-Ti	MobileNetV3 Small[:13]
Vim-S	MobileNetV3 Large[:17]
VideoMamba-Ti	MobileNetV3 Small[:13]

A Architecture Details

Our **DART** requires a small pretrained feature extractor to obtain general image features for region score prediction. Specifically, the feature extractors used by each model listed in the main paper are summarized in Table 5.

B Qualitative Analysis

In this section we present segmentation visualizations on several images from the ImageNet-1K validation set selected by our model to facilitate qualitative analysis. (9)

C Additional Experiments

For hybrid-architecture networks that contain convolutions or their variants, we experimented with modifying our patch partitioning strategy: instead of the irregular grid proposed in the main paper, we apply a *non-uniform regular grid*, and after resampling we stitch the resulting patches back into image form before feeding them into the backbone. This approach is straightforward and requires no change to the backbone; simply inserting our module before the backbone is sufficient. However, compared with the partitioning method proposed in the main text, the regular grid offers less flexibility and therefore yields lower performance, serving only as a simple attempt for convolutional networks.

We conducted a brief experiment on the recently published **RMT**, whose architecture is broadly similar to Swin but whose stem consists of several convolutional layers; each stacked block includes convolutional positional embeddings (CPE) and relies on convolutions for down-sampling. The *L* variant achieves state-of-the-art performance within 100 M parameters without extra supervision or data. The results show that, after simply inserting our module, it reaches **85.7%** ImageNet-1K top-1 validation accuracy (+0.2%) with only 210 training epochs (a 30% reduction).

Figure 10 uses a simple example to illustrate the limitations of the non-uniform regular grid compared with the method proposed in the main paper.

Our DART module decouples the token sequence length fed into the backbone from the input image resolution. As a result, changing the resolution no longer affects FLOPs. In practice, increasing the input resolution only improves the clarity of patches that are smaller than the average size. As shown in Figure 11, our approach benefits from higher input resolutions, indicating that the performance gain indeed originates from the densely partitioned regions with higher local resolution.

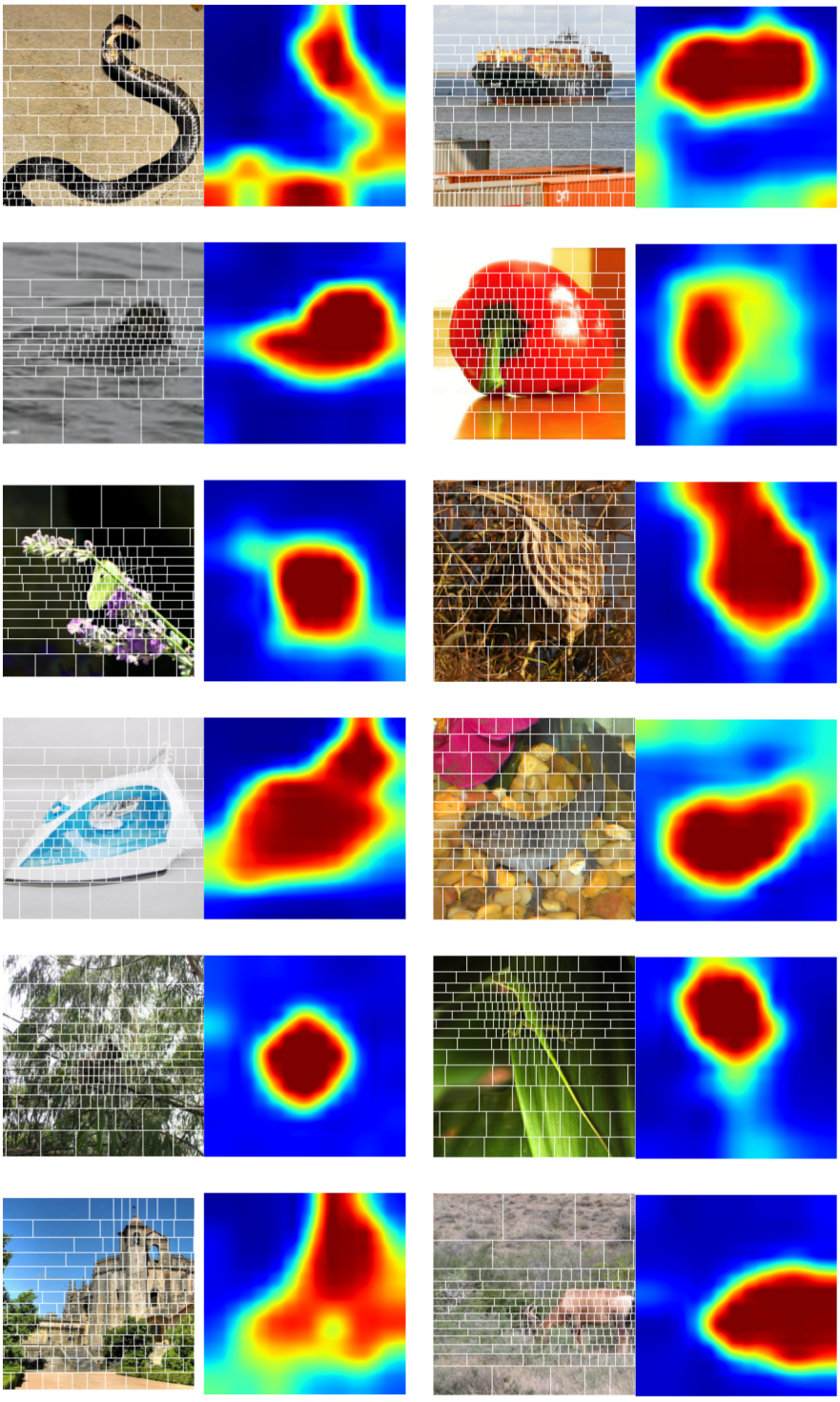

Figure 8: partitions examples produced by our model.

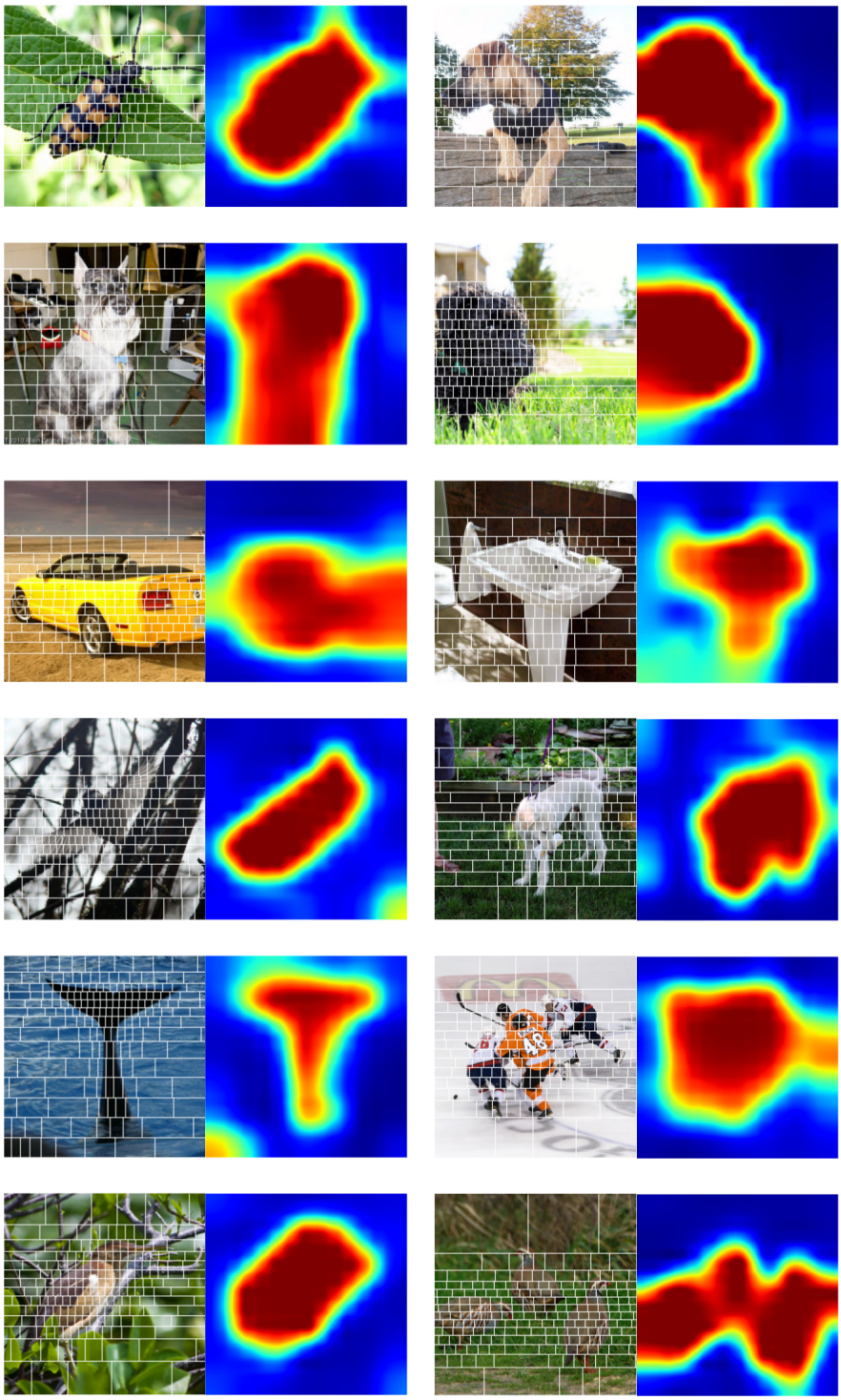

Figure 9: partitions examples produced by our model.

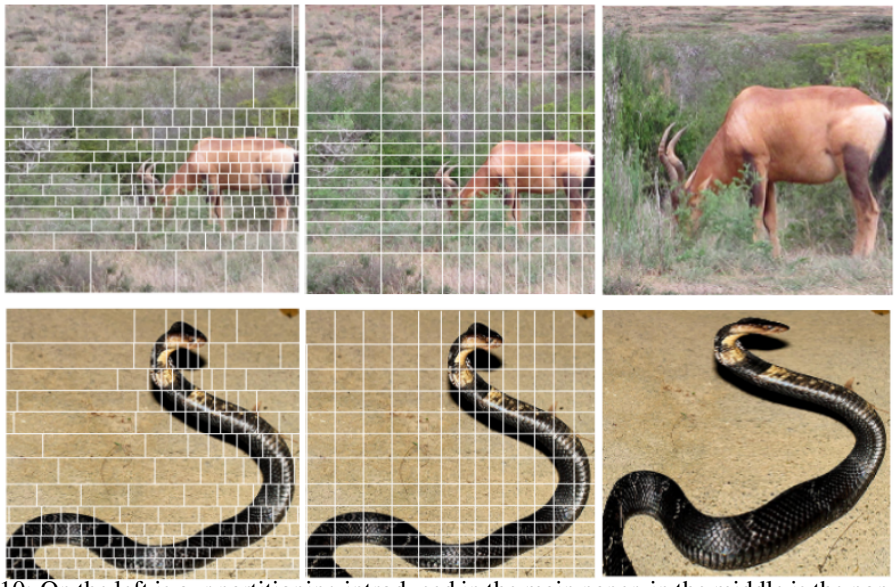

Figure 10: On the left is our partitioning introduced in the main paper, in the middle is the non-uniform regular grid partitioning, on the right is the reassembled image.

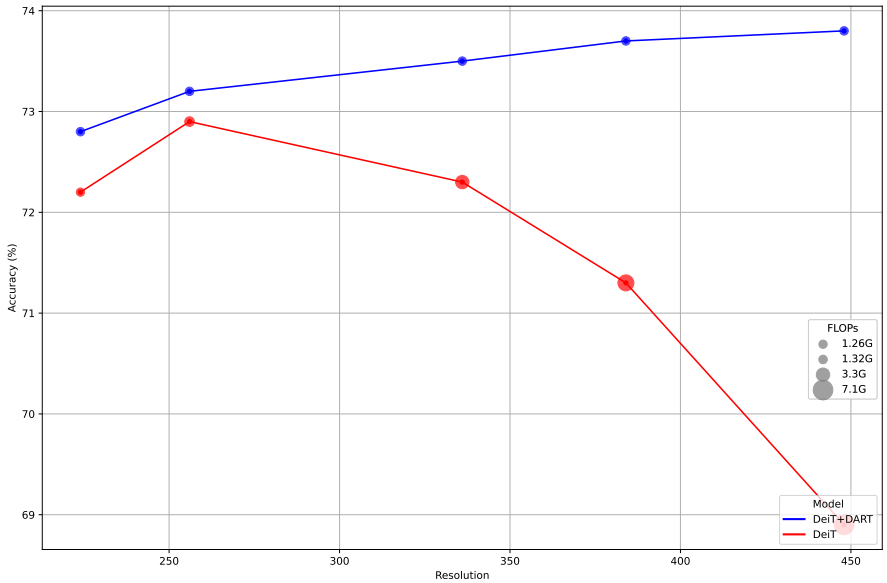

Figure 11: Accuracy vs. input resolution and computational cost.